Journal of
Alzheimer's Disease & Parkinsonism

Hashimoto et al., J Alzheimers Dis Parkinsonism 2018, 8:2
DOI: 10.4172/2161-0460.1000433

Research Article Open Access

Mitochondrial Complex I Deficit in the Olfactory Systems of Age-related Neurodegenerative Monkey Models: A PET Study using ^{18}F-BCPP-EF

Fumio Hashimoto, Hiroyuki Ohba, Masakatsu Kanazawa, Shingo Nishiyama, Takeharu Kakiuchi and Hideo Tsukada*

Central Research Laboratory, Hamamatsu Photonics K.K., Hamamatsu, Shizuoka 434-8601, Japan

Abstract

Objective: Dysfunction of olfactory bulb area (OBA) is reported in several types of neurodegenerative diseases such as Alzheimer's disease and Parkinson's disease. Although pathophysiological mechanisms responsible for changes in olfactory function remain unclear, the quantitative parameters for olfactory function are expected for diagnose of neurodegenerative diseases. We developed a novel probe for positron emission tomography (PET), ^{18}F-2-tert-butyl-4-chloro-5-{6-[2-(2-fluoroethoxy)-ethoxy]-pyridin-3-ylmethoxy}-2H-pyridazin-3-one (^{18}F-BCPP-EF), for quantitative analysis of mitochondrial complex I (MC-I) activity in the living brain. In the present study, the applicability of ^{18}F-BCPP-EF to predict age-related neurodegenerative damage in the monkey brain as an MC-I deficit in the OBA was investigated.

Methods: PET measurements with ^{11}C-PiB for amyloid--β (Aβ), ^{11}C-DPA-713 for translocator protein (TSPO) and ^{18}F-BCPP-EF were performed in aged monkeys. The binding specificity of ^{18}F-BCPP-EF to MC-I in the OBA was evaluated with rotenone, a specific MC-1 inhibitor, in young animals. ^{11}C-PiB binding to Aβ and ^{11}C-DPA-713 binding to TSPO were calculated as standard uptake value ratios (SUVRs). The total distribution volume (V_T) of ^{18}F-BCPP-EF was calculated using a Logan graphical analysis using metabolite-corrected plasma input function, and correlations between the olfactory V_T of ^{18}F-BCPP-EF and SUVRs of ^{11}C-PiB or ^{11}C-DPA-713 in several brain regions were analyzed.

Results: Pre-dosing of rotenone resulted in the significant reduction of V_T values in all brain regions including the OBA. MC-I activity in the OBA exhibited age-related reduction, which positively correlated with MC-I activity in the olfactory-related and cortical regions. OBA MC-I and TSPO as measured using ^{11}C-DPA-713 were inversely correlated in the olfactory-related and cortical regions, but association between OBA MC-I and Aβ deposition as measured using ^{11}C-PiB were observed only in olfactory-related regions.

Conclusion: The present study demonstrated that OBA MC-I activity could be a potential predictive parameter of neurodegenerative damages related Aβ deposition and TSPO/neuroinflammation in the living brain.

Keywords: Aging; Brain; Olfactory bulb; Mitochondrial complex I; Amyloid-β; Neuroinflammation; PET

Introduction

Olfactory ability to correctly identify a smell was previously reported to be defective not only in the course of physiologically normal aging but also in the patients with Alzheimer's disease, Parkinson's disease, and Huntington's disease [1-4]. University of Pennsylvania smell identification test (UPSIT) has been applied to assess olfactory function and clinical reports using behavioral testing showed a correlation between cognitive status and baseline olfactory test scores in the elderly, those with mild cognitive impairment (MCI), and patients with Alzheimer's disease [5,6]. In contrast, most cases of preclinical Alzheimer's disease have no subjective symptoms of olfactory dysfunction, suggesting a poor understanding of the prevalence of olfactory dysfunction in the normally aging population and those with related diseases [7].

Previous studies indicated that neurodegenerative diseases target specific networks in the brain, and connectivity within brain networks may partly explain the spread of neurodegeneration. The olfactory system and connected areas provide a neural network that may be involved in selective network-driven neuronal vulnerability in relation to a neurodegenerative Alzheimer's disease-related pathology, suggesting that the olfactory system has potential as a diagnostic index of Alzheimer's disease. The pathophysiological mechanisms responsible for changes in olfactory function currently remain unclear; however, previous studies were conducted on Alzheimer's disease patients in order to elucidate these mechanisms using positron emission tomography (PET) [8-10]. PET applied target-oriented PET probes for the quantitative imaging of specific target molecules related to Alzheimer's disease, such as the cholinergic system, amyloid-β (Aβ) and tau deposition in the brains of patients with Alzheimer's disease. Furthermore, we anticipated PET probes that may provide more general indices of brain function [11-14]. One useful indicator may be the regional cerebral metabolic rate of glucose (rCMRglc) using ^{18}F-fluoro-2-deoxy-D-glucose (^{18}F-FDG) for the PET imaging of neurodegenerative damage; however, this probe has some limitations. ^{18}F-FDG was taken up into not only normal brain tissues, but also inflammatory regions with microglial activation in the sub-acute phase after transient focal ischemia in the brains of rodents and monkeys [15-18]. Recent studies demonstrated the involvement of neuroinflammation with microglial activation in several neurodegenerative disorders suggesting that this property results in the underestimation of neurodegenerative damage by FDG-PET [19-22].

In order to resolve this issue with ^{18}F-FDG, we designed a novel PET

***Corresponding author:** Hideo Tsukada, Central Research Laboratory, Hamamatsu Photonics K.K. 5000 Hirakuchi, Hamakita, Shizuoka 434-8601, Japan, Tel: +81-53-586-7111; Fax: +81-53-586-8075; E-mail: tsukada@crl.hpk.co.jp

Received March 23, 2018; **Accepted** March 26, 2018; **Published** April 02, 2018

Citation: Hashimoto F, Ohba H, Kanazawa M, Nishiyama S, Kakiuchi T, et al. (2018) Mitochondrial Complex I Deficit in the Olfactory Systems of Age-related Neurodegenerative Monkey Models: A PET Study using ^{18}F-BCPP-EF. J Alzheimers Dis Parkinsonism 8: 433. doi: 10.4172/2161-0460.1000433

probe, ^{18}F-2-tert-butyl-4-chloro-5-{6-[2-(2-fluoroethoxy)-ethoxy]-pyridin-3-ylmethoxy}-2H-pyridazin-3-one (^{18}F-BCPP-EF), to image mitochondrial complex I (MC-I) function [23]. MC-I is the first enzyme of the respiratory electron transport chain in living cells. In vitro assessment using isolated mitochondria confirmed the specificity of BCPP-EF and its related compounds to MC-I, and the specific binding of ^{18}F-BCPP-EF to MC-I was also confirmed by pre-administration of rotenone, a specific MC-I inhibitor, in the living brain [17,24,25]. ^{18}F-BCPP-EF-PET detected ischemic neuronal damage 7 days after an ischemic insult by which time higher ^{18}F-FDG uptake was observed in the damaged area because of microglial activation [16-18]. Our findings demonstrated 1-methyl-4-phenyl-1,2,3,6-tetrahydropyridine (MPTP)-induced diffuse reductions in ^{18}F-BCPP-EF binding to MC-I throughout the brain, not only in dopaminergic neurons in the nigrostriatal regions but also in presynaptic serotonergic neurons in the cortex [26,27]. Significant age-related reductions in MC-I activity were detected in the living brains of monkeys, and MC-I activity in the cortex of aged monkeys inversely correlated with the deposition of Aβ, measured using ^{11}C-PiB, and neuroinflammation, measured using ^{11}C-DPA-713 [21].

In the present study, changes in MC-I activity in the olfactory bulb area (OBA) of the living brains of monkeys (*Macaca mulatta*) were measured using ^{18}F-BCPP-EF in order to assess its potential as a parameter for age-related neurodegenerative damage. The specificity of ^{18}F-BCPP-EF binding to MC-1 was evaluated by the pre-administration of rotenone, a specific MC-1 inhibitor, in young animals. Age-related effects on MC-I activity in the OBA were evaluated in the living brains of young and aged monkeys. Furthermore, the connectivity of MC-I activity between the OBA and olfactory-related and cortical regions and the relationship between an MC-I deficit in the OBA and Aβ deposition or neuroinflammation in the olfactory-related and cortical regions were examined.

Materials and Methods

Anatomical definition

The olfactory bulb area (OBA) means the olfactory bulb from the adjacent gyrus rectus of the frontal base. The olfactory related area includes hippocampus, amygdala and hypothalamus.

Animals and drugs

Ten young male (3-5 years old) and 10 aged male (20-24 years old) rhesus monkeys (*Macaca mulatta*) were used for the PET measurements. Magnetic resonance images (MRI) of monkeys were obtained with a 3.0 T MR imager (Allegra; Siemens, Erlangen, Germany) under pentobarbital anesthesia.

Rotenone and the precursor of ^{11}C-PiB were obtained from Sigma-Aldrich Japan (Tokyo, Japan) and PharmaSynth (Tartu, Estonia), respectively. The standard compound of PiB was from ABX Advanced Biochemical Compounds (Radeberg, Germany). The precursors of ^{11}C-DPA-713, ^{18}F-BCPP-EF and their corresponding standard compounds were purchased from NARD Institute Ltd. (Amagasaki, Japan).

PET ligands syntheses

Positron-emitting carbon-11 (^{11}C) and fluorine-18 (^{18}F) were produced by ^{14}N(p, α)^{11}C and ^{18}O(p, n)^{18}F nuclear reactions, respectively, using the cyclotron (HM-18, Sumitomo Heavy Industry, Ltd., Tokyo, Japan) at the Hamamatsu Photonics PET center. Labeled compounds were synthesized using a modified CUPID system (Sumitomo Heavy Industries, Ltd., Tokyo, Japan). HPLC analyses of labeled compounds were performed on a GL-7400 low-pressure gradient HPLC system (GL Sciences, Inc., Tokyo, Japan) with a radioactivity detector (RLC-700, Hitachi Aloka Medical, Inc., Tokyo, Japan).

^{11}C-PiB was synthesized by the *N*-methylation of nor-compound *N*-desmethyl-PiB with ^{11}C-methyl triflate. Radiochemical purity was more than 96% and specific radioactivity was 36.7 ± 10.1 GBq/μmol. ^{11}C-DPA-713 was synthesized by the *N*-methylation of nor-compound *N*-desmethyl-DPA with ^{11}C-methyl triflate. Radiochemical purity was more than 99% and specific radioactivity was 99.3 ± 32.2 GBq/μmol. ^{18}F-BCPP-EF for MC-I was prepared by the nucleophilic ^{18}F-fluorination of the corresponding precursor as reported previously [23]. Radiochemical purity was more than 99% and specific radioactivity was 58.9 ± 7.9 GBq/μmol.

Drug treatments

In order to assess the binding specificity of ^{18}F-BCPP-EF to MC-I, rotenone, an MC-1 inhibitor, in 0.5 mL/kg of *N*, *N*-dimethylformamide/polyethylene glycol 400/saline (1:1:2) was infused into monkeys through a posterior tibial vein cannula for 1h, and ^{18}F-BCPP-EF was then injected as a bolus into monkeys for PET measurement [17,25].

PET measurements in monkey brain

Almost all PET scans were conducted for measurements under conscious states, as reported previously [21,25,27]. After overnight fasting, a venous cannula for the PET ligand injection and an arterial cannula for blood sampling were inserted in both inferior limbs. The animal's head was rigidly fixed to the upper frame of a monkey chair using an acrylic head-restraining device. The animal sitting in the restraining chair was placed at a fixed position in the PET gantry with stereotactic coordinates aligned parallel to the orbito-meatal plane.

For PET measurements under anesthetic state in 4 young control and 4 young rotenone-treated animals, PET scans were conducted as reported previously [18]. Since our previous study confirmed no significant anesthetic effects of isoflurane on ^{18}F-BCPP-EF binding to MC-I in the living monkey brain both conscious and anesthetized data were analyzed together [21]. After overnight fast, monkeys were sedated with 5 mg/kg i.m. of ketamine, intubated, immobilized with 0.05 mg/kg/h i.v. of pancuronium bromide, and artificially ventilated (Cato, Drager, Germany). Anesthesia was continued with 0.8 vol. % isoflurane in a N_2O/O_2 (2:1) gas mixture during the entire experiment. A venous cannula for PET ligand injection and an arterial cannula for blood sampling were inserted in both inferior limbs. The mean arterial blood pressure, heart rate, rectal temperature, arterial PO_2 and PCO_2 and pH were continuously or regularly monitored. During the experiments, the animal's body temperature was maintained within normal limits with heating blankets. The animal was set in a supine position on a bed with head holder (SFCT-RB-PR-2, Hamamatsu Photonics, Hamamatsu, Japan) was placed at a fixed position in the PET gantry with stereotactic coordinates aligned parallel to OM plane.

After a transmission scan for 30 min using a ^{68}Ge-^{68}Ga rotation rod source, a dynamic emission scan for 91 min with each PET probe was conducted using an animal PET scanner (SHR-7700, Hamamatsu Photonics, Hamamatsu, Japan). The PET data obtained were reconstructed by the FBP method with a Hanning filter of 4.5 mm FWHM and attenuation correction using transmission scan data. Individual PET and MRI images were co-registered. Volumes of interest (VOIs) in brain regions were drawn manually on MRI with reference to

regional information from BrainMaps.org and the VOIs of MRI were superimposed on co-registered PET images in order to measure the time activity curves of each PET probe for kinetic analyses [28]. In order to avoid excessive stress on animals, arterial blood sampling was only performed in scans with ^{18}F-BCPP-EF.

PET data analysis

In the quantitative analysis of ^{18}F-BCPP-EF, arterial blood samples were obtained every 8 sec up to 64 sec, followed by 90 and 150 sec, and then 4, 6, 10, 20, 30, 45, 60, 75 and 90 min after the tracer injection, and blood samples were centrifuged to separate plasma, weighed, and their radioactivity was measured. In the metabolite analysis, methanol was added to some plasma samples (sample/methanol=1/1) obtained 16, 40, and 64 s and 6, 10, 30, 45, 60, 75 and 90 min after the injection, followed by centrifugation. The supernatants obtained were developed with thin layer chromatography plates (AL SIL G/UV, Whatman, Kent, UK) with a mobile phase of ethyl acetate. The ratio of the unmetabolized fraction was assessed using a phosphoimaging plate (FLA-7000, Fuji Film, Tokyo, Japan). The input function of unmetabolized ^{18}F-BCPP-EF was calculated using data obtained by corrections of the ratio of the unmetabolized fraction to total radioactivity, which was used as the arterial input function. Kinetic analyses of ^{18}F-BCPP-EF were performed by a Logan graphical analysis using PMOD software (PMOD Technologies Ltd., Zurich, Switzerland) [29].

In analyses of ^{11}C-PIB for Aβ deposition and ^{11}C-DPA-713 for translocator protein (TSPO) activity, PET images were normalized by the injected dose and the subject weight to produce standardized uptake value (SUV) images. Then, SUV images averaged from 60 to 90 min and from 40 to 60 min, respectively, after the injection were created, and VOIs were set on each SUV image with the aid of MRI of individual monkeys. SUV ratios (SUVR) of each region (SUV (region)) against SUV in the cerebellum (SUV (cerebellum)) were calculated [30].

Statistical analysis

Results are expressed as means ± SD. Comparisons between conditions were carried out using the paired, two-tailed Student's t-test. A probability level of less than 5% ($p<0.05$) was considered to indicate statistical significance.

Results

Figure 1 shows typical PET/MRI fusion images of ^{18}F-BCPP-EF-PET (A-C), ^{11}C-PiB (D) and ^{11}C-DPA-713 (E) from young (A and B) and aged (C-E) monkeys.

In the quantitative analysis of MC-1 activity using ^{18}F-BCPP-EF, a Logan graphical analysis was applied for total distribution volume (V_T) image generation and regional V_T value calculations, and the effects of rotenone and aging on MC-I activity were assessed in the living monkey brain. Logan-V_T values were the highest in the occipital cortex, higher in the parietal cortex, intermediate in the hippocampus, amygdala, hypothalamus, and frontal and temporal cortices, and the lowest in the OBA of young normal monkeys (Figure 2). As shown in Figures 1A, 1B and 2, the pre-administration of rotenone, a specific MC-1 inhibitor, at a dose of 0.1 mg/kg/h markedly reduced V_T values in olfactory-related

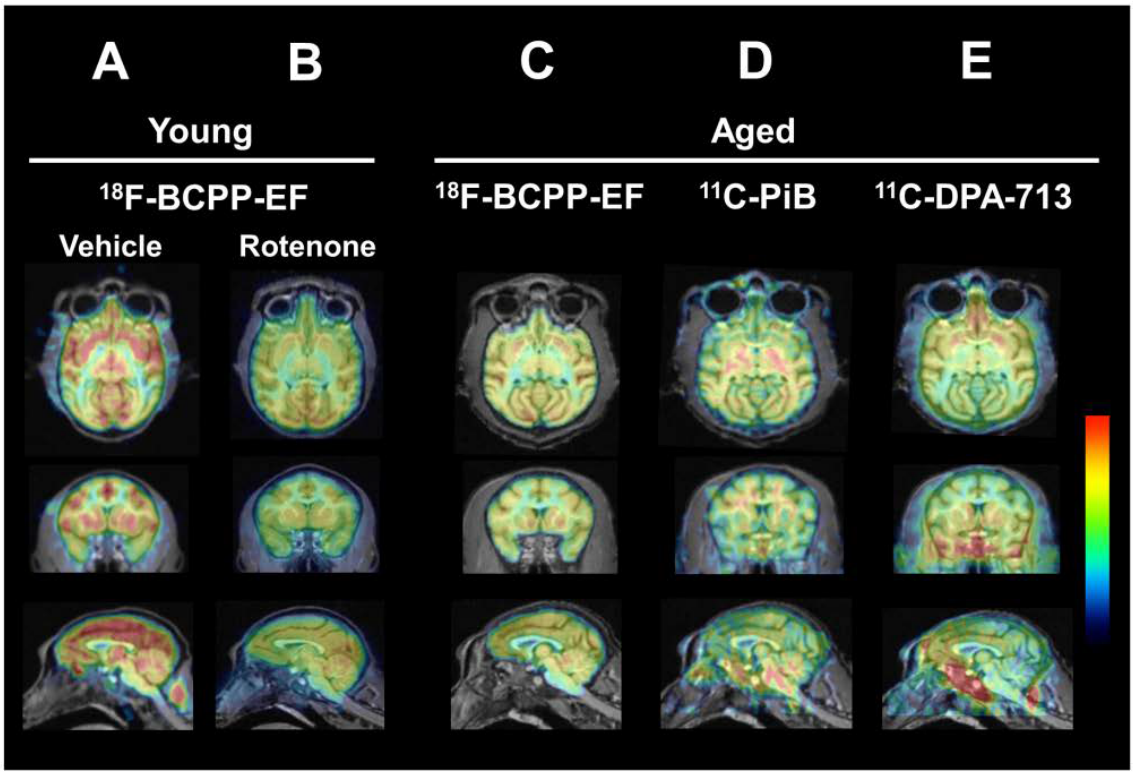

Figure 1: Typical PET/MRI fusion images of ^{18}F-BCPP-EF-PET (A-C), ^{11}C-PiB (D) and ^{11}C-DPA-713 (E) in young (A and B) and aged (C-E) monkeys (*Macaca mulatta*). After the infusion of vehicle (A and C) or rotenone at 0.1 mg/kg/h (B) for 1 h, PET scans were conducted for 91 min after the ^{18}F-BCPP-EF injection with sequential arterial blood sampling. The binding of ^{18}F-BCPP-EF to MC-1 was calculated using a Logan graphical analysis with metabolic-corrected plasma input. After 91 min of PET measurements using ^{11}C-PiB or ^{11}C-DPA-713 in aged monkeys, Aβ deposition and TSPO were assessed as SUV ratios using the cerebellum as a reference region.

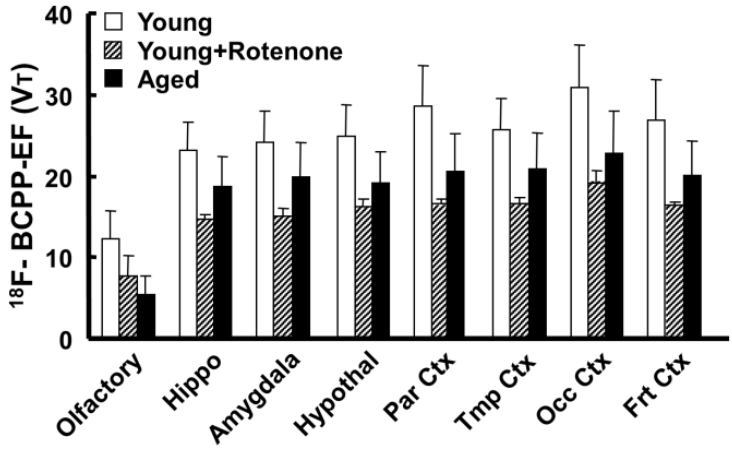

Figure 2: Effects of rotenone and aging on V_T of ^{18}F-BCPP-EF in living brains of monkeys (*Macaca mulatta*). After the infusion of vehicle or rotenone at 0.1 mg/kg/h for 1 h, PET scans were conducted for 91 min after the ^{18}F-BCPP-EF injection. Arterial blood samples were sequentially obtained to assess metabolite-corrected arterial plasma input for the Logan graphical analysis. ROIs were set on reconstructed PET images to obtain TACs. Data are expressed as the mean ± SD for 10 animals. * p<0.05 vs. "Young" for each corresponding region.

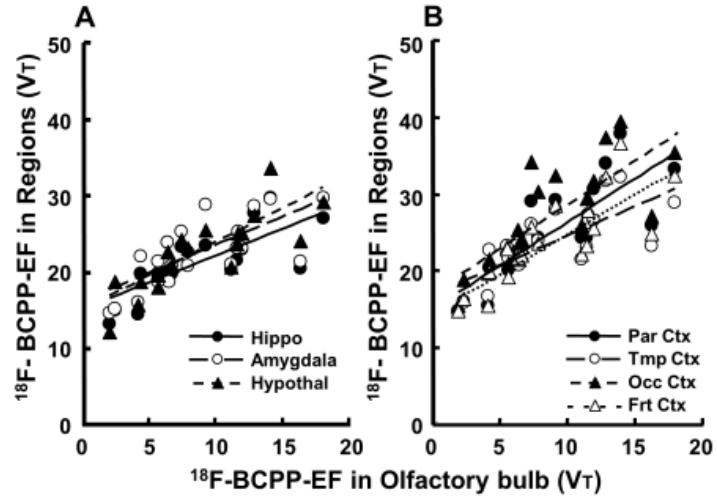

Figure 3: Correlations of the V_T of ^{18}F-BCPP-EF in olfactory-related regions (hippocampus, amygdala, and hypothalamus) (A) or cortical regions (parietal, temporal, occipital and frontal cortices) (B) against the V_T of ^{18}F-BCPP-EF in the olfactory bulb area of living brains of young and aged monkeys.

(hippocampus, amygdala, and hypothalamus; average=60.3% of the vehicle condition) and cortical regions (parietal, temporal, occipital, and frontal cortices; 58.1%) including the OBA (59.9%). Aged animals had significantly lower V_T values in olfactory-related (average=79.8% of young) and cortical regions (75.5%) than those in young animals (Figure 2). It is important to note that aging effects on MC-I activity were the most prominent in the OBA, being 44.7% in young animals (Figure 2).

In order to examine regional interactions in MC-I activity between the OBA and several brain regions, correlation analyses were performed using V_T values in the olfactory-related and cortical regions of young and aged animals. The plotting results obtained demonstrated that the regional V_T values of ^{18}F-BCPP-EF in olfactory-related (hippocampus r^2=0.561; amygdala r^2=0.536; hypothalamus r^2=0.676, P<0.01 in all areas) and cortical regions (parietal r^2=0.672; temporal r^2=0.545; occipital r^2=0.614; frontal r^2=0.662; P<0.01 in all areas) correlated well with the V_T values of the OBA in living monkey brains (Figures 3A and 3B).

When the regional SUVR of ^{11}C-PiB was plotted against the V_T values of ^{18}F-BCPP-EF in the OBA of aged animals, the results obtained indicated an inverse relationship, with correlations being observed between OBA MC-I and Aβ deposition in the hippocampus (r^2=0.800, P<0.01), amygdala (r^2=0.563, P<0.01) and hypothalamus (r^2=0.572, P<0.01) (Figure 4).

The plot of the regional SUVR of ^{11}C-DPA-713 against the V_T values of ^{18}F-BCPP-EF in the OBA of aged animals revealed an inverse relationship, showing correlations between OBA MC-I and neuroinflammation in all olfactory-related regions (hippocampus r^2=0.930; amygdala r^2=0.928; hypothalamus r^2=0.550, P<0.01 in all areas) (Figure 5A) and all cortical regions (parietal r^2=0.871; temporal r^2=0.651; occipital r^2=0.496, frontal r^2=0.662; P<0.01 in all areas) (Figure 5B).

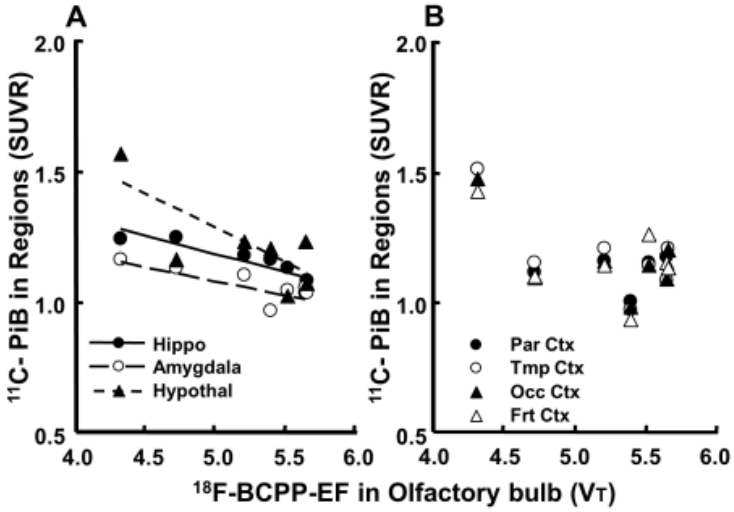

Figure 4: Correlations of the SUVR of ^{11}C-PiB in olfactory-related regions (hippocampus, amygdala and hypothalamus) (A) or cortical regions (parietal, temporal, occipital and frontal cortices) (B) against the V_T of ^{18}F-BCPP-EF in the olfactory bulb area of living brains of aged monkeys.

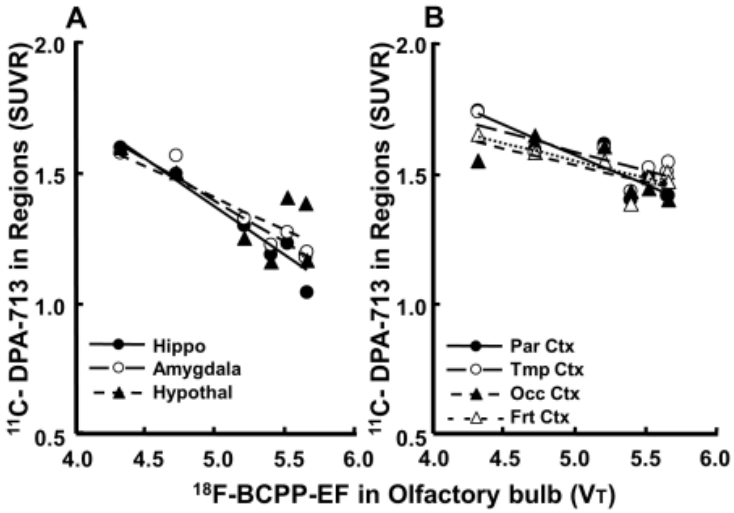

Figure 5: Correlations of the SUVR of ^{11}C-DPA-713 in olfactory-related regions (hippocampus, amygdala and hypothalamus) (A) or cortical regions (parietal, temporal, occipital, and frontal cortices) (B) against the V_T of ^{18}F-BCPP-EF in the olfactory bulb area of living brains of young and aged monkeys.

Discussion

This is the first study to demonstrate that OBA MC-I activity measured using ^{18}F-BCPP-EF-PET could be a potential predictive parameter of neurodegenerative damages related Aβ deposition and TSPO/neuroinflammation in the living brains of aged nonhuman primate (*Macaca mulatta*) using animal PET.

The present study showed the suppression of ^{18}F-BCPP-EF uptake by the pre-administration of rotenone, a specific MC-I inhibitor, in all brain regions analyzed, including the OBA, with uptake being inhibited to a similar extent in all regions. Although a dose-escalation study for full displacement was not performed because of the lethal effects of rotenone on cardiac function, significant reductions in V_T were observed even at a relatively low dose of 0.1 mg/kg/h, suggesting that the uptake of ^{18}F-BCPP-EF reflected specific binding to MC-I, even in the OBA.

The present study confirmed our previous findings that ^{18}F-BCPP-EF detected the age-related reduction of MC-1 activity in the all cortical regions of living monkey brain using PET [25]. Mitochondrial respiratory chain failures have been implicated as factors in the aging process, and this is called the "mitochondrial free radical theory of aging" [31]. Increases in the production of mitochondrial reactive oxygen species (ROS) with aging are regarded as toxic byproducts of aerobic metabolism that induce oxidative damage to various cellular macromolecules. Mitochondria are the main intracellular source of ROS and also the main target of oxyradical-mediated damage and cumulative free radical damage, leading to significant changes in brain mitochondrial function. Since MC-I is an important factor in the regulation of mitochondrial respiration as well as a source of ROS in mitochondria, we previously demonstrated that assessments of MC-I activity using ^{18}F-BCPP-EF may be useful for the detection of age-related changes in cortical function, which may be involved in the age-related memory impairment in monkeys [21,25,32].

Furthermore, the remarkable finding of the present study was that age-related reductions in MC-I activity were observed also in the OBA in a group comparison between young and aged animals. The extent of reductions in MC-I activity in the OBA was significantly greater than those in any other brain regions. This result is consistent with previous findings showing that patients progressing to Alzheimer's disease showed the greater loss of gray matter than MCI patients remaining stable, and this loss mainly occurred in the olfactory network [33]. Olfactory ability has been reported to become defective in the course of physiologically normal aging and olfactory dysfunction occurs even before the clinical presentation of Alzheimer's disease [1,6]. In patients with Alzheimer's disease, the olfactory system and areas with extensive connections to this system exhibit several pathological changes. Collectively, these results suggest that specific and sensitive parameters of OBA function, such as MC-I activity, are useful as predictors of preclinical Alzheimer's disease.

In assessments of the OBA in aged animals, Aβ deposition, a pathological hallmark of Alzheimer's disease, measured using ^{11}C-PiB did not reflect the MC-I deficit assessed with ^{18}F-BCPP-EF-PET, which is consistent with previous findings of a weak relationship between UPSIT performance and Aβ deposition in the OBA [8,10]. Inconsistent findings have been reported in postmortem studies; some studies did not detect Aβ deposition in the OBA, while others showed the presence of Aβ in the OBA, mostly in severe Alzheimer's disease patients [34-36]. In contrast, the deposition of hyperphosphorylated tau, another pathological hallmark of Alzheimer's disease, in the OBA was more consistent than the presence of Aβ deposition [35,36]. Mitochondrial transport along microtubules within axons is crucial for axonal maintenance, and its dysregulation by hyperphosphorylated tau may contribute to neurodegenerative diseases [37]. Therefore, it may be more useful to assess the deposition of hyperphosphorylated tau in the OBA of the living brain, as previously elucidated using ^{18}F-Flortaucipir and PET [9].

Several *in vivo* imaging studies reported a weak relationship between UPSIT performance and cortical Aβ deposition; however, an *in vivo* imaging study using functional MRI revealed that blood oxygen level-dependent signal activation induced by a lavender oil odorant in the primary olfactory cortex and hippocampus correlated with UPSIT in MCI and AD patients [8,10,38]. In order to ensure the capability of OBA MC-I as a predictive parameter of neurodegenerative damage in cortical regions, correlation analyses were performed between MC-I activity in the OBA and those in olfactory-related and cortical regions. The combined data of young and aged animals revealed positive correlations between MC-I activity in the OBA and those in olfactory-related and cortical regions. These findings suggested strong connectivity between the OBA and olfactory-related and cortical regions.

When the relationship between OBA MC-I activity, measured using ^{18}F-BCPP-EF, and regional Aβ deposition, measured using ^{11}C-PiB, was investigated in aged monkeys, inverse correlations were observed in olfactory-related regions (hippocampus, amygdala, and hypothalamus), but not in cortical regions. Previous studies reported that no species other than humans show marked neuron loss or cognitive decline approaching clinical grade AD in humans, and aged monkeys did not exhibit as high Aβ deposition and ^{11}C-PiB uptake in cortical regions as those reported in AD patients. The present results support the histopathological finding that cortical Aβ deposition was not directly linked with olfactory ability; however, ^{11}C-PiB does not directly measure the more toxic soluble forms of Aβ, which disrupt neural network function [21,39-41]. If direct measurements of soluble Aβ were performed, a clearer relationship between OBA MC-I activity and cortical Aβ deposition may have been found.

In the correlation analysis in the OBA, TSPO activity, as a neuroinflammation marker, measured using ^{11}C-DPA-713, showed an inverse relationship with the MC-I deficit assessed using ^{18}F-BCPP-EF. Furthermore, when the relationship between OBA MC-I activity and regional neuroinflammation was evaluated, inverse correlations were noted in all olfactory-related regions (hippocampus, amygdala, and hypothalamus) as well as all cortical regions (parietal, temporal, occipital, and frontal cortices). TSPO activity measured using ^{11}C-DPA-713 was sufficiently high for correlation analyses, even in the limited sample size of aged monkeys used in the present study. In mammalian species, the olfactory system has strong connections with several brain regions, such as the hippocampus and neocortical areas that are related to memory function and display AD pathology. The inverse correlation observed between OBA MC-I and TSPO in olfactory-related and cortical regions and the positive correlations between OBA MC-I and MC-I olfactory-related and cortical regions are mirror-image relationships; both support our working hypothesis that MC-I assessments in the OBA may be useful for investigating connectivity and activity in the spread of pathology in AD.

The present study had a few limitations. Due to the limited sample size of aged animals, a replicative study with a larger sample may be required for more definite conclusions, particularly regarding the relationship between OBA MC-I activity and cortical Aβ deposition measured as low-level ^{11}C-PiB uptake. In addition, since this study included only resting-state MC-I activity, the task-based MC-I imaging of olfactory responses may provide important insights into early changes in olfaction.

Conclusion

The present study demonstrated that OBA MC-I activity measured using ^{18}F-BCPP-EF-PET has potential as a predictive parameter of neurodegenerative damage related to Aβ deposition, as measured using ^{11}C-PiB, and TSPO/neuroinflammation, as measured using ^{11}C-DPA-713, in the living brain. Further studies on the relationship between OBA MC-I activity and olfactory ability assessed by UPSIT need to be performed in order to confirm the capability of ^{18}F-BCPP-EF-PET for the preclinical detection of AD.

Acknowledgement

We gratefully acknowledge the technical assistance provided by Aiko Iwazaki, Dai Fukumoto and Norihiro Harada.

References

1. Doty RL (2009) The olfactory system and its disorders. Semin Neurol 29: 74-81.
2. Velayudhan L (2015) Smell identification function and Alzheimer's disease: A selective review. Curr Opin Psychiatry 28: 173-179.
3. Doty RL (2012) Olfactory dysfunction in Parkinson disease. Nat Rev Neurol 8: 329-339.
4. Barresi M, Ciurleo R, Giacoppo S, Foti Cuzzola V, Celi D, et al. (2012) Evaluation of olfactory dysfunction in neurodegenerative diseases. J Neurol Sci 323: 16-24.
5. Doty RL, Shaman P, Dann M (1984) Development of the University of Pennsylvania smell identification test: A standardized microencapsulated test of olfactory function. Physiol Behav 32: 489-502.
6. Masurkar AV, Devanand DP (2014) Olfactory dysfunction in the elderly: Basic circuitry and alterations with normal aging and Alzheimer's disease. Curr Geriatr Rep 3: 91-100.

7. Bahar-Fuchs A, Moss S, Rowe C, Savage G (2011) Awareness of olfactory deficits in healthy aging, amnestic mild cognitive impairment and Alzheimer's disease. Int Psychogeriatr 23: 1097-1106.

8. Bahar-Fuchs A, Chetelar G, Villemagne VL (2010) Olfactory deficits and amyloid-β burden in Alzheimer's disease, mild cognitive impairment and healthy aging: A PiB PET study. J Alzheimers Dis 22: 1081-1087.

9. Risacher SL, Tallman EF, West JD, Yoder KK, Hutchins GD, et al. (2017) Olfactory identification in subjective cognitive decline and mild cognitive impairment: Association with tau but not amyloid positron emission tomography. DADM 9: 57-66.

10. Vassilaki M, Christianson TJ, Mielke MM, Geda YE, Kremers WK, et al. (2017) Neuroimaging biomarkers and impaired olfaction in cognitively normal individuals. Ann Neurol 81: 871-882.

11. Kadir A, Nordberg A (2010) Target-specific PET probes for neurodegenerative disorders related to dementia. J Nucl Med 51: 1418-1430.

12. Morris E, Chalkidou A, Hammers A, Peacock J, Summers J, et al. (2016) Diagnostic accuracy of ^{18}F amyloid PET tracers for the diagnosis of Alzheimer's disease: A systematic review and meta-analysis. Eur J Nucl Med Mol Imaging 43: 374-385.

13. Barthel H, Sabri O (2017) Clinical use and utility of amyloid imaging. J Nucl Med 58: 1711-1717.

14. Dani M, Brooks DJ, Edison P (2016) Tau imaging in neurodegenerative diseases. Eur J Nucl Med Mol. Imaging 43: 1139-1150.

15. Meles SK, Teune LK, de Jong PM, Dierckx RA, Leenders KL (2017) Metabolic imaging in Parkinson disease. J Nucl Med 58: 23-28.

16. Schroeter M, Dennin MA, Walberer M, Backes H, Neumaier B, et al. (2009) Neuroinflammation extends brain tissue at risk to vital peri-infarct tissue: A double tracer [^{11}C]PK11195- and [^{18}F]FDG-PET study. J Cereb Blood Flow Metab 29: 1216-1225.

17. Tsukada H, Nishiyama S, Fukumoto D, Kanazawa M, Harada N (2014) Novel PET probes ^{18}F-BCPP-EF and ^{18}F-BCPP-BF for mitochondrial complex I: A PET study by comparison with ^{18}F-BMS-747158-02 in rat brain. J Nucl Med 55: 473-480.

18. Tsukada H, Ohba H, Nishiyama S, Kanazawa M, Kakiuchi T, et al. (2014) PET imaging of ischemia-induced impairment of mitochondrial complex I function in monkey brain. J Cereb Blood Flow Metab 34: 708-714.

19. Winkeler A, Boisgard R, Martin A, Tavitian B (2010) Radioisotopic imaging of neuroinflammation. J Nucl Med 51: 1-4.

20. Jacobs AH, Tavitian B, INMiND consortium (2012) Noninvasive molecular imaging of neuroinflammation. J Cereb Blood Flow Metab 32: 1393-1415.

21. Tsukada H, Nishiyama S, Ohba H, Kanazawa M, Kakiuchi T, et al. (2014) Comparing amyloid-β deposition, neuroinflammation, glucose metabolism and mitochondrial complex I activity in brain: A PET Study in aged monkeys. Eur J Nucl Med Mol Imaging 41: 2127-2136.

22. Brendel M, Probst F, Jaworska A, Overhoff F, Korzhova V, et al. (2016) Glial activation and glucose metabolism in a transgenic amyloid mouse model: a triple-tracer PET study. J Nucl Med 57: 954-960.

23. Harada N, Nishiyama S, Kanazawa M, Tsukada H (2013) Development of novel PET probes, [^{18}F]BCPP-EF, [^{18}F]BCPP-BF and [^{11}C]BCPP-EM for mitochondrial complex 1 imaging in the living brain. J Labeled Comp Radiopharm 56: 553-561.

24. Kazami S, Nishiyama S, Kimura Y, Itoh H, Tsukada H (2018) BCPP compounds, PET probes for early therapeutic evaluations, specifically bind to mitochondrial complex I. Mitochondrion S1567-7249.

25. Tsukada H, Ohba H, Kanazawa M, Kakiuchi T, Harada N (2014) Evaluation of ^{18}F-BCPP-EF for mitochondrial complex I imaging in conscious monkey brain using PET. Eur J Nucl Med Mol Imaging 41: 755-763.

26. Tsukada H, Kanazawa M, Ohba H, Nishiyama S, Harada N, et al. (2016) PET imaging of mitochondrial complex I with ^{18}F-BCPP-EF in brain of Parkinson's disease model monkey. J Nucl Med 57: 950-953.

27. Kanazawa M, Ohba H, Nishiyama S, Kakiuchi T, Tsukada H (2017) Effects of MPTP on serotonergic neuronal systems and mitochondrial complex I activity in the living brain: A PET study on conscious rhesus monkeys. J Nucl Med 58: 1111-1116.

28. Jones EG, Stone JM, Karten HJ (2011) High-resolution digital brain atlases: A Hubble telescope for the brain. Ann NY Acad Sci 1225: E147-E159.

29. Logan J, Fowler JS, Volkow ND, Wolf AP, Dewey SL, et al. (1990) Graphical analysis of reversible radioligand binding from time-activity measurements applied to [N-^{11}C-methyl]-(-)-cocaine PET studies in human subjects. J Cereb Blood Flow Metab 10: 740-747.

30. Price JC, Klunk WE, Lopresti BJ, Lu, X, Hoge JA, et al. (2005) Kinetic modeling of amyloid binding in humans using PET imaging and Pittsburgh Compound-B. J Cereb Blood Flow Metab 25: 1528-1547.

31. Bratic A, Larsson NG (2013) The role of mitochondria in aging. J Clin Invest 123: 951-957.

32. Tsukada H, Nishiyama, S, Fukumoto D, Ohba H, Sato K, et al. (2004) Effects of Acute acetylcholinesterase inhibition on the cerebral cholinergic neuronal system and cognitive function: Functional imaging of the conscious monkey brain using animal PET in combination with microdialysis. Synapse 52: 1-10.

33. Prestia A, Drago V, Rasser PE, Bonetti M, Thompson PM, et al. (2010) Cortical changes in incipient Alzheimer's disease. J Alzheimer Dis 22: 1339-1349.

34. Struble RG, Clark HB (1992) Olfactory bulb lesions in Alzheimer's disease. Neurobiol Aging 13: 469-473.

35. Christen-Zaech S, Kraftsik R, Pillevuit O, Kiraly M, Martins R, et al. (2003) Early olfactory involvement in Alzheimer's disease. Can J Neurol Sci 30: 20-25.

36. Attems J, Walker L, Jellinger KA (2014) Olfactory bulb involvement in neurodegenerative diseases. Acta Neuropathol 127: 459-475.

37. Su B, Wang X, Zheng L, Perry G, Smith MA, et al. (2010) Abnormal mitochondrial dynamics and neurodegenerative diseases. Biochim Biophys Acta 1802: 135-142.

38. Wang J, Eslinger PJ, Doty RL, Zimmerman EK, Grunfeld R, et al. (2010) Olfactory deficit detected by fMRI in early Alzheimer's disease. Brain Res 1357: 184-194.

39. Finch CE, Austad SN (2012) Primate aging in the mammalian scheme: The puzzle of extreme variation in brain aging. Age 34: 1075-1091.

40. Wilson RS, Arnold SE, Schneider JA, Tang Y, Bennett DA (2007) The Relationship between cerebral Alzheimer's disease pathology and odor identification in old age. J Neurol Neurosurg Psychiatry 78**:** 30-35.

41. Shankar GM, Le S, Mehta TH, Garcia-Munoz A, Shepardson NE, et al. (2008) Amyloid β-protein dimers isolated directly from Alzheimer brains impair synaptic plasticity and memory. Nat Med 14**:** 837-842.